FATIGUE CRITERION FOR SHORT FIBER REINFORCED THERMOPLASTIC (PA66 GF50) OVER A WIDE RANGE OF LOAD RATIOS

P. Santharam[a, b], Y. Marco[b], V. Le Saux [b], M. Le Saux [b], I. Raoult [d], G. Robert [c], P. Charrier [a], D. Taveau [a]

a. Vibracoustic, CAE and Durability Prediction Department, 44474 Carquefou, France.
b. ENSTA Bretagne, UMR CNRS 6027, IRDL, 29200 Brest, France.
c. Solvay Engineering Plastics, 69457 Lyon, France.
d. PSA Peugeot Citroën, Direction Scientifique et des Technologies futures, Route de Gisy, 78943 Vélizy-Villacoublay, cedex, France.

Abstract:

Composites of polyamide matrix reinforced by short glass fibers are increasingly used as replacement for metal parts in the automotive industry, especially because they are light weighted and easy to manufacture. Automobile parts are usually subjected to fatigue loadings during their service life, which makes it necessary to have a reliable or predictable durability life. Short glass fiber reinforced (SGFR) thermoplastics are used in structural parts such as top strut and motor mounts wherein they are subjected to complex positive and negative loads. As they are injection-molded, they exhibit a complex fiber orientation distribution, which clearly has an effect on their mechanical properties. Moreover, the polyamide matrix in SGFR thermoplastics is sensitive to ambient humidity and temperature. Therefore, a fatigue criterion for this material should unify different load ratios, fiber orientation distributions for the given atmospheric conditions. In literature, a wide variety of fatigue criteria has been proposed; nevertheless, single unified fatigue criterion yet has space for improvement. This article proposes an energy-based fatigue criterion that tends to take into account a load ratio and fibers orientation effects.

Keywords: PA66GF50, Fatigue, Energy Criterion, Creep Energy

1 Introduction

Fig. 1. Injection molding SGFR thermoplastic part.

The recent success of the short glass fiber reinforced (SGFR) thermoplastics over metal parts among automotive manufacturers is due to their durability resistance and their lower weight (~50% than metal parts), accounting also with reduced price. Thanks to the injection molding process, complex automobile parts with multiple ribs such as motor mounts are made possible, as illustrated in Fig. 1. The motor mounts made in SGRF polyamide 6.6 (PA66) consist of a mounting bracket and a supporting arm that are responsible to transfer/reduce the vibrations produced by the motor into a damping element. These motor mounts are subjected to complex cyclic loading conditions, including tension and compression, and are exposed to temperatures around 80°C and humidity ratios of approximately 50%. Their resistance to fatigue in such conditions is thus an important issue. Furthermore, due to the injection molding process, SGFR thermoplastic parts show a

complex fiber orientation distribution which has an effect on their mechanical properties. A unified fatigue energy criterion which could be applied to various loading ratios and could consider both the complex anisotropic microstructure and thermomechanical behavior of the material is needed. Among several energy-based criteria in the literature, the dissipated energy criterion based on infra-red (IR) temperature measurements is relevant for PA66 thermoplastics reinforced with 50 wt. % of glass fibers (PA66-GF50) [1-5].

In this article, we propose to take into account the load ratio effect by considering Creep Energy (W_{creep}), which is introduced in this paper, Dissipated Energy (Δ^*) deduced from IR measurements and Hysteresis Loop Energy (ΔE_h) for PA66GF50 (50% of glass fibers). Here, the material is exposed to atmospheric conditions reading 50% humidity and 80°C temperature (RH50 T80°C). In section 2, the geometry description of the sample, the experimental procedures and the database are presented. In section 3, fatigue lifetime indicators are discussed along with their evolution during the cycling. In the final section, we discuss about the formulation of possible fatigue criteria which are capable of predicting the fatigue lifetime according to the database presented in section 2.

2 Experimental procedure

2.1 Material and samples

The PA66GF50, provided by Solvay is the used material. The dimensions of the injection molded 3mm-thick plate are shown in Fig. 1. The line gate and flow length are optimized to provide planar orientation of the specimen. The useful region is carefully selected making sure it is neither too close nor too far from the gate. The dog-bone specimens are machined from this plate so that their main loading direction during the tests are oriented at 0°, 45° and 90° from the injection direction, as shown in Fig.1. Due to injection molding process, the material shows a heterogeneous microstructure. In particular, a strong through-thickness gradient of fibers orientation is observed (this gradient is also referred as "skin-core" effect in literature) [6, 7].

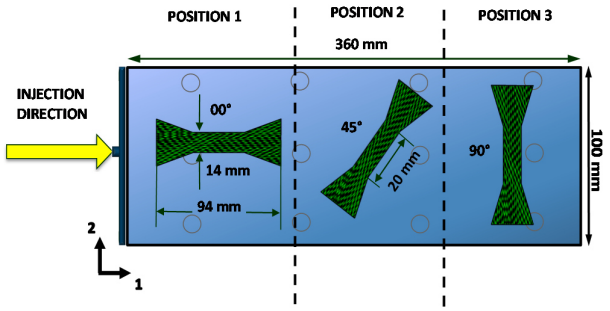

Fig. 2. Injection molding of dog-bone samples.

2.2 Experimental set-up

The tests were performed at Solvay Engineering Plastic, France. The atmospheric condition experienced by the motor mount during its lifetime is approximated to be RH50 T80°C. Since the material is sensitive to humidity and temperature [8], the above-mentioned atmospheric conditions (RH50 T80°C) were maintained during the tests, thanks to a Weiss climatic chamber. Two servo hydraulic machines (MTS 319.02 and MTS 370.10) were used to perform classical cyclic fatigue tests until failure. Either a contact extensometer or digital image correlation (DIC) based on images obtained from a 3D optical camera were used to measure the displacements within the sample gauge part and then to calculate the strain. To provide the contrast needed two correlate images, a random speckle patterns was applied by black and white paints sprays. The strains obtained from DIC and from the contact extensometer gave similar results for dog bone sample in fatigue test. Temperature fields at the surface of the specimen in the climatic chamber were measured using a FLIR X6540SC camera. For the IR measurements, the

variations of the atmosphere in the chamber were taken into account by subtracting the temperature experienced by a virgin specimen placed inside the chamber to the temperature of the loaded sample. The entire experimental set-up is shown in Fig. 3. The IR camera and the 3D optical camera were synchronized to capture images only for specific cycles to limit the size of the database.

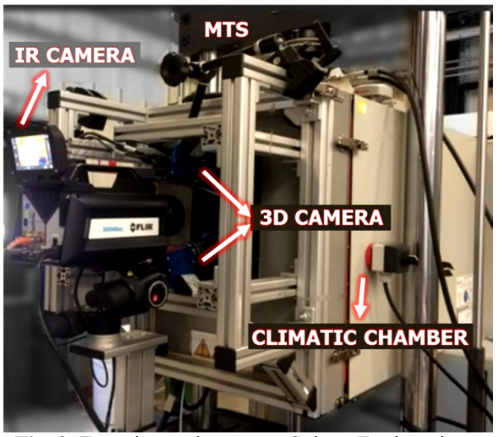

Fig. 3. Experimental set-up at Solvay Engineering Plastics, France.

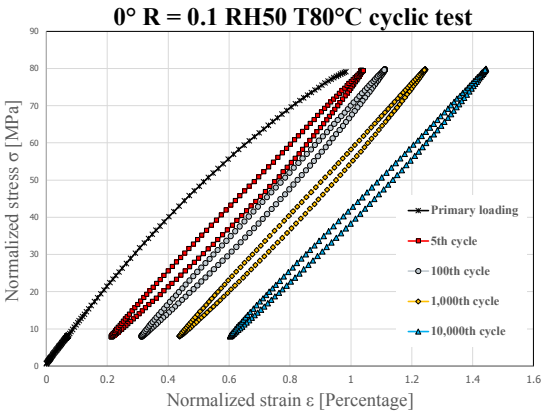

Fig. 4. Hysteresis cycles during a fatigue test.

2.3 Database at RH50@T80°C

The entire extensive database consists of 343 classical fatigue tests with various load ratios R (0.7, 0.5, 0.3, 0.1, -0.2, -0.5), with approximately 58 tests (0°, 45°, and 90° orientations included) for each load ratio. All the tests were conducted at 3Hz frequency. Only five cycles were recorded for each log base 10 cycles increment during the test. An example of normalized engineering nominal stress versus strain plot is shown in Fig. 4 for a 0°-oriented sample, for a load ratio of 0.1. Mechanical phenomena such as strain ratcheting associated with reduction of the area of the hysteresis loop between loading and unloading are noticed as the number of cycles increases.

The following thermomechanical data can be obtained for each recorded cycle:

- Minimum, maximum values and evolution of local (Green-Lagrange) strain, ε;
- Minimum and maximum temperature values, $\theta = T - T_0$.

In turn, this gives access to the evolutions of the following characteristics as a function of the number of cycles:

- The secant modulus, E_s;
- The elastic energy, ΔE_t;
- The hysteresis loop energy, ΔE_h;
- The dissipated energy obtained from IR measurement, Δ^* [1].

In this paper, we focus only on ΔE_h, Δ^* and the creep energy defined in section 3.2 (W_{creep}). All the graphs presented in this article are normalized for confidentiality purpose.

3 Fatigue lifetime indicators

3.1 Hysteresis loop energy

The hysteresis loop energy (ΔE_h) is the area of the loop observed on the nominal stress-strain curves, as shown in Fig. 4. The evolution of the hysteresis loop energy against the number of cycles is shown below in Fig. 5, wherein one example is plotted for each orientation (0°, 45° and 90°) and each load ratio (0.7, 0.5, 0.3, 0.1, -0.2 and -0.5). In most cases the stabilization occurs within the first few cycles. Nevertheless, for some tests, especially for load ratios of 0.1 and below, the evolution fluctuates before reaching the stabilization point. In the same graph, vertical lines are used to indicate the location of mid-life (half of the number of cycles to failure). On closer observations, it is evident that for all the tests, the stabilization of the hysteresis loop is almost reached after 10 cycles.

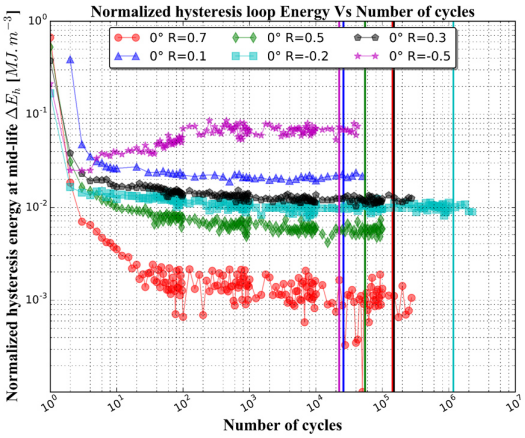

Fig. 5. Hysteresis loop energy vs number of cycles.

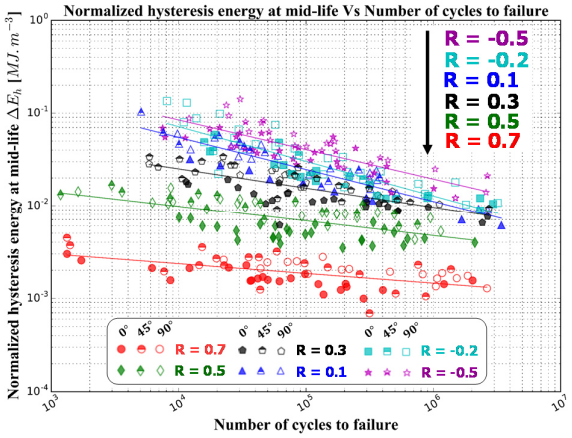

Fig. 6. Hysteresis loop energy vs number of cycles to failure.

Therefore, values of ΔE_h at mid-life are plotted against number of cycles to failure in Fig. 6, for the different tested load ratios and sample orientations. For all tested load cases, ΔE_h does not depend on the orientation of the sample. In addition, solid lines in Fig. 6 indicate the power law fit obtained for the different load ratios. Furthermore, the parameters of the power law follow a logical ranking order as a function of the load ratio between R = -0.5 and R = 0.7, as shown in Fig. 6. It appears that the hysteresis loop energy has the ability to group the data obtained for negative load ratios (-0.5, -0.2) and R = 0.1 to certain extent, showing larger dissipation than for positive load ratios (0.5 and 0.7).

3.2 Creep energy

The purpose of the creep energy (W_{creep}) is to find a relation between creep and mean-stress in order to account for the load ratio effect. As shown in Fig. 7, the minimum and maximum strains measured/calculated in the region of interest either by DIC or contact extensometer continuously increase during cycling until failure. No direct correlation was observed between the fatigue life and the minimum strain (ε_{min}), the maximum strain (ε_{max}) or the mean strain (ε_{mean}) values. In order to include the effect of creep, equation (1) is used to express the mean strain increment during one cycle as function of its corresponding cycle, as illustrated in Fig. 7. This strain increment was calculated for all the recorded cycles in the test (except for the first and last cycles). The evolution of the strain increment as a function of the number of cycles is shown in Fig. 8 along with the corresponding power law fit, for each load ratio (0.7, 0.5, 0.3, 0.1, -0.2, -0.5), with 0°-orientation.

$$V_{creep} = \frac{d\left(\frac{1}{2}(\varepsilon_{max} - \varepsilon_{min})\right)}{dN} \quad (1)$$

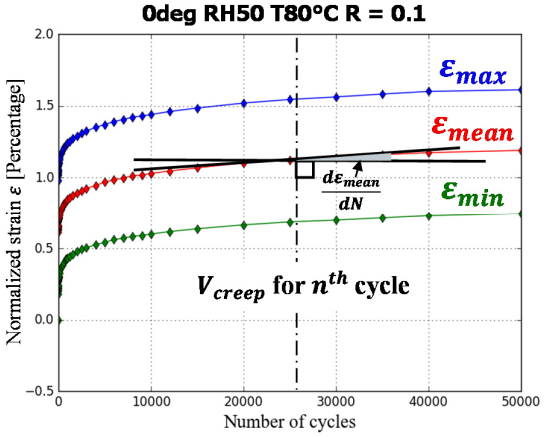

Fig. 7. Normalized strain vs number of cycles.

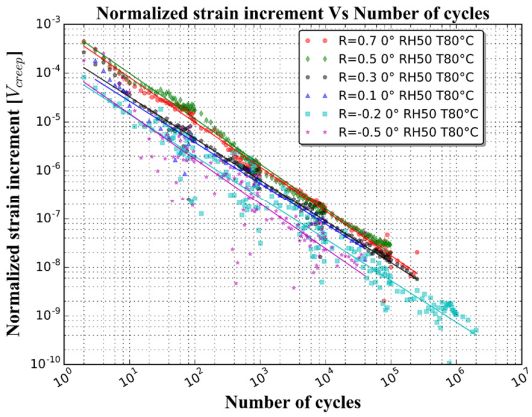

Fig. 8. Normalized strain increment vs number of cycles.

V_{creep} is then calculated by using a power law fit for all the tests in equation (1). In consistency with the analysis presented in section 3.1, mid-life value of V_{creep} is plotted against the number of cycles to failure in Fig. 9, for the various sample orientations and load ratios tested.

On one hand, as observed for ΔE_h against number of cycles to failure (Fig. 6), mid-life V_{creep} does not depend on the orientation of the sample (Fig. 9). On the other hand, in contrary to ΔE_h, V_{creep} is able to group data for most of the positive load ratios (0.7, 0.5, 0.3) and load ratio R = 0.1 up to certain extent. Indeed, a logical ranking order is noticed as a function of the load ratio (Fig. 9), as observed for ΔE_h, while it is reversed (Fig. 6).

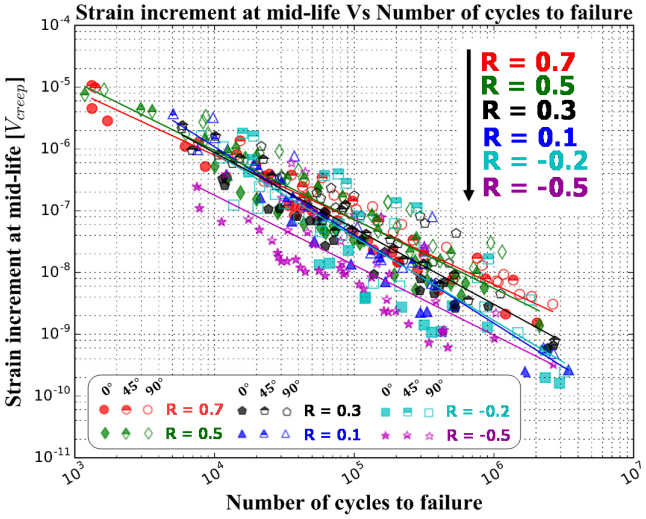

Fig. 9. Normalized strain increment vs number of cycles.

In order to compare strain increment indicator with other indicators such as ΔE_h, the following expression (equation (2)) is proposed to calculate the so-called creep energy (W_{creep}) from V_{creep}, where σ_{mean} is the mean stress.

$$W_{creep} = \sigma_{mean} * V_{creep} \quad (2)$$

3.2 Dissipated energy

The robustness of dissipated energy (Δ^*) calculation using heat build-up protocol for the cyclic tests was shown in the literature for PA66-GF50 [2, 3]. Fig. 10 shows the evolution of mean temperature of the sample during cycling, for the 0°-orientation case (one test illustrated for each load ratio). The mean

temperature tends to stabilize after a few hundreds of cycles. The intrinsic dissipated energy per cycle (Δ^*) is calculated using the mean stabilized temperature $\overline{\theta_{mean}}$ and characteristic time τ as in equation (3).

$$\Delta^* = \frac{\rho C_p}{f} * \frac{\overline{\theta_{mean}}}{\tau} \quad (3)$$

Where ρ the density of PA66GF50, C_p is its heat capacity C_p properties of and f is the loading frequency. $\overline{\theta_{mean}}$ and τ are identified for all the tests by fitting the sample mean temperature data measured using the IR camera with the expression given in equation (4) where t is time, assuming that the mean temperature has a stabilization point. This assumption is reasonable only if the cyclic heat source (dissipation energy) is constant during the test. This hypothesis is consistent with the results presented in section 3.1 and Fig. 5. The fits obtained are shown in Fig. 10.

$$\theta_{mean} = \overline{\theta_{mean}}\left(1 - e^{-\left(\frac{t-t_0}{\tau}\right)}\right) \quad (4)$$

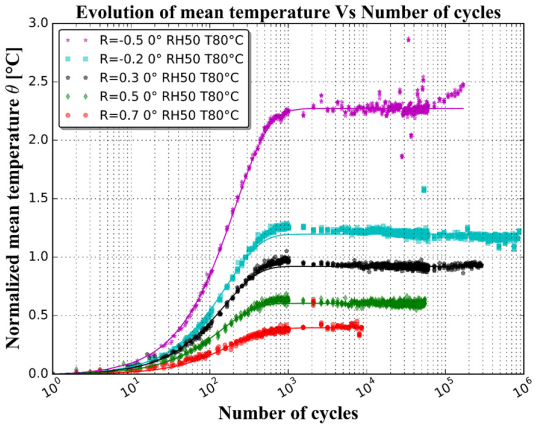

Fig. 10. Evolution of mean temperature vs number of cycles.

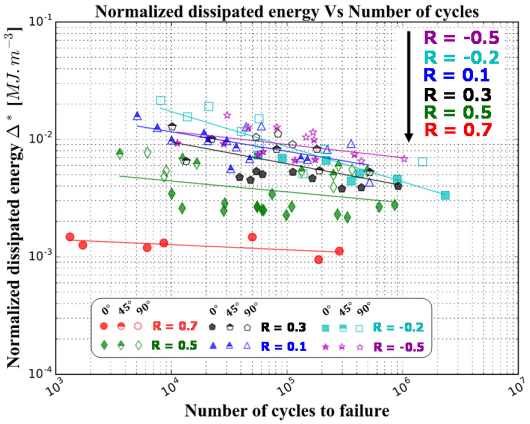

Fig. 11. Dissipated energy vs number of cycles to failure.

Δ^* was calculated for 102 tests equipped with IR camera, for load ratios (0.7, 0.5, 0.3, 0.1, -0.2 and -0.5) and orientations (0°, 45° and 90°) combined. The obtained values of Δ^* are plotted against number of cycles to failure for the various sample orientations and load ratios in Fig.11. Similarly to ΔE_h in section 3.1, Δ^* does not depend on the orientation of the sample. Moreover, grouping is observed for the negative load ratios, similarly to the observations made forΔE_h. In Fig. 12, ΔE_h is plotted against Δ^* for its corresponding tests, for all the tests discussed in Fig. 11.

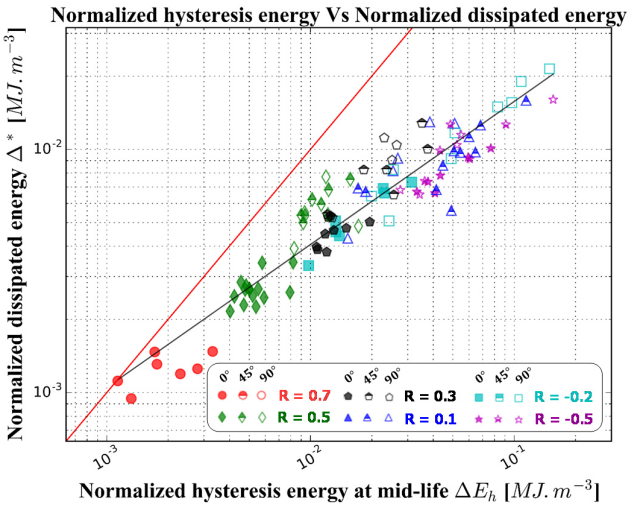

Fig. 12. Dissipated energy vs hysteresis loop energy.

The hysteresis loop area observed during fatigue test is related to the viscoelastic and/or (visco) plastic nature of the material [2, 8]. Energy dissipated by the hysteresis loops (ΔE_h) is not completely turned

into heat or dissipated energy (Δ^*) as shown in equation (5), where dissipated energy is D_1 and hysteresis loop energy is W'_{def}, and W'_s, W'_e are stored energy and elastic energy respectively [9,10]. In accordance with this equation, Fig. 12 shows that only a fraction of the hysteresis loop energy is turned into dissipation (~58%).

$$W'_s = W'_{def} - W'_e - D_1 \tag{5}$$

4 Fatigue criterion

The purpose is to determine a fatigue criterion efficient over a wide range of load ratios, by combining two of the energy indicators discussed in section 3. First, Δ^* is combined to W_{creep} according to equation (6), where $A_{creep}, A_{diss}, a_{creep}, a_{diss}$ are the parameters to be identified on the basis of the database including 102 tests results, in order to predict the number of cycles to failure N_r.

Fig. 13 compares experimental and predicted number of cycles to failure. The solid blue line indicates perfect prediction and the red and the blue regions respectively represent errors of half and full decades away from the blue line. The agreement between experimental and predicted number of cycles to failure is satisfactory.

Second, Δ^* in equation (6) is replaced by ΔE_h to obtain equation (7) where $A_{creep}, A_{hys}, a_{creep}, a_{hys}$ are the parameters to be identified.

$$\frac{1}{N_r} = \left(\frac{W_{creep}}{A_{creep}}\right)^{a_{creep}} + \left(\frac{\Delta^*}{A_{diss}}\right)^{a_{diss}} \tag{6}$$

$$\frac{1}{N_r} = \left(\frac{W_{creep}}{A_{creep}}\right)^{a_{creep}} + \left(\frac{\Delta E_h}{A_{hys}}\right)^{a_{hys}} \tag{7}$$

The parameters were identified on the basis of 343 tests with different orientations and load ratios. The experiment against predicted number of cycles to fatigue is shown in Fig. 14. A satisfactory correlation is observed. A majority of the tests are within the acceptable region of error (red region – half decade error). On the whole, only few points, for negative load ratios (-0.2 and -0.5), are above one-decade error.

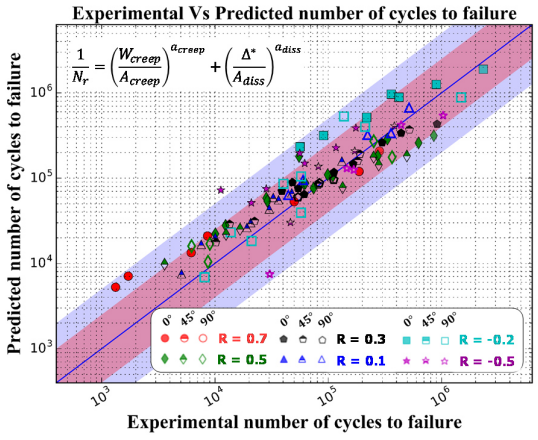

Fig. 13. Dissipated energy and creep energy criterion.

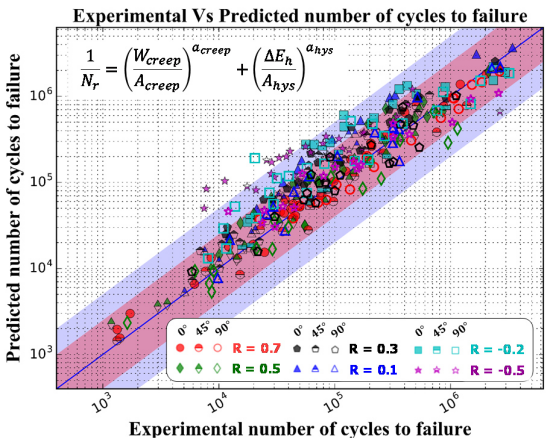

Fig. 14. Hysteresis loop energy and creep energy criterion.

4 Conclusions

A wide database of fatigue tests, including various load ratios (between -0.5 and +0.7) and loading directions with respect to the injection direction (0, 45 and 90°), was derived for PA66GF50 at RH50 T80°C. Three types of energy calculations are presented for prediction of fatigue lifetime: hysteresis loop energy ΔE_h, creep energy W_{creep} and dissipated energy Δ^*. Grouping between negative load ratios is possible using ΔE_h and Δ^* as criteria. W_{creep} allows grouping between positive load ratios. By combining W_{creep} with ΔE_h or Δ^* in a criterion, it is possible to predict the fatigue lifetime for both positive and negative load ratios.

Though prediction of fatigue lifetime for PA66GF50 has already been achieved by different energy-based criterion in the literature, grouping for wide range of load ratios was not yet addressed. The proposed criterion has opened possibilities to challenge this issue, by proposing a criterion able to group a wide range of load ratios for various loading directions from the injection direction.

References

[1] Le Saux V., Marco Y., Calloch S., Doudard C., Charrier P., Fast evaluation of the fatigue lifetime of rubber-like materials based on a heat build-up protocol and micro-tomography measurements, International Journal of fatigue, 32(10) (2010) 1582–1590.
[2] Launay A., Maitournam M.H., Marco Y., Raoult I., Multiaxial fatigue models for short glass fiber reinforced polyamide, Part II: Fatigue life estimation, International Journal of Fatigue, 47 (2013) 390-406.
[3] Jegou L., Marco Y., Le Saux V., Calloch S., Fast Prediction of the Wöhler curve from heat build-up measurements, International Journal of fatigue, 47 (2013) 259-267.
[4] SerranoAbello L., Marco Y., Le Saux V., Robert G., Charrier P., Fast Prediction of the Fatigue Behavior of Short Fiber Reinforced Thermoplastics from Heat Build-up Measurements, Procedia Engineering, 66 (2013), 737-745.
[5] Marco Y., Le Saux V., Jégou L., Launay A., Serrano L., Raoult I., Calloch S., Dissipation analysis in SFRP structural samples: Thermomechanical analysis and comparison to numerical simulations, International Journal of fatigue, 67 (2014) 142–150.
[6] Santharam P., Parenteau T., Charrier P., Taveau D., Le Saux V., Marco Y., Complex fibers orientation distribution evaluation in short glass fiber-reinforced thermoplastic (PA66 GF50), In : 12th International Fatigue Congress, Poitiers (France) 2018.
[7] Bay R.S., Tucker III C.L., Stereological measurement and error estimation for three-dimentional fiber orientation, Polymer Engineering & Science, 32(4) (1992), 240-253, 317, 332.
[8] Leveuf L., Navrátil L., Le Saux V., Marco Y., Olhagaray J., Leclercq S., Constitutive equations for the cyclic behaviour of short carbon fibre-reinforced thermoplastics and identification on a uniaxial database, Continuum Mechanics and Thermodynamics,
[9] Benaarbia A., Chrysochoos A., Robert G., Thermomechanical behavior of PA6.6 composites subjected to low cycle fatigue, Composites Part B, 76 (2015) 52-64, (2018), 1-18.
[10] Bernasconi A., Davoli P., Basile A., and Filippi A., Effect of fibre orientation on the fatigue behaviour of a short glass fibre reinforced polyamide-6, International Journal of Fatigue, 29 (2007) 199-208.